ELSEVIER

Clinical Biomechanics 17 (2002) 64–72

CLINICAL BIOMECHANICS

www.elsevier.com/locate/clinbiomech

Mechanical conditions in the internal stabilization of proximal tibial defects

Georg N. Duda *, Francesco Mandruzzato, Markus Heller, Jean-Pierre Kassi, Cyros Khodadadyan, Norbert P. Haas

Research Laboratory, Trauma and Reconstructive Surgery, Humboldt University of Berlin, Campus Virchow-Klinikum, Augustenburger Platz 1, Charité, 13353 Berlin, Germany

Received 7 February 2001; accepted 16 October 2001

Abstract

Objectives. The goal was to design a method which would permit an assessment of the suitability of a newly developed implant under physiological-like loading conditions. Information obtained from such an analysis is expected to delineate more clearly the indications for a new device prior to clinical utilization.

Design. In vitro mechanical stiffness testing and finite element analysis.

Methods. From in vitro testing of proximal tibiae with defects, the stiffness of an internal stabilization system was determined. Using a finite element model, the loading of both the implant and bone was analyzed including all muscle forces. The variation in implant loading and interfragmentary strain for different defect locations was also investigated.

Results. Conventional stiffness testing demonstrated the comparability of the experimental findings with the finite element predictions. Under physiological-like loading the implant experienced high bending and von Mises stresses if defects in the region of the shaft were stabilized. A short working length increased implant loading up to the yield strength of the material.

Conclusions. The finite element analysis illustrated the appropriateness of this new device for proximal defects of the tibia, but the implant should be used hesitantly in fractures or defects extending into the diaphyseal region of the bone.

Relevance

This new analytical approach helped to identify clinical indications for the implant in which its mechanical attributes would prove advantageous. © 2002 Elsevier Science Ltd. All rights reserved.

Keywords: Proximal tibial defect; Internal fixator; Bone healing; Physiological-like loading

1. Introduction

Nail, plate and external fixator have for decades been the most frequently used stabilizers for the surgical treatment of dia- and metaphyseal defects. They have been greatly improved in recent years and their indications have been broadened [1]. The choice of the osteosynthesis device has thereby become an issue of special interest since the local mechanical properties associated with the fixation may influence the process of bone healing [2]. The mechanical environment generated in defect situations provides an essential stimulus for bone formation [2,3] and affects the healing rate [4].

In this respect, the stiffness of the fixation system has a substantial effect on the healing process [5]. This especially holds true in bone defect situations in which load is not transferred through the defect ends but solely through the implant itself. A change in bone loading after osteosynthetic stabilization is indeed expected on the local as well as on the global level. Extensive sections of the bone may be subjected to un- or overloading leading to bone resorption and remodeling [6]. Within the fixation system, high stresses and fatigue due to repetitive loading can lead to its technical failure. A better understanding of the loading of the implant as well as the strain distribution within the bone will certainly help improve understanding of the mechanical aspects of the biological healing process. Furthermore, a thorough comprehension of the loading of implant and bone is essential when selecting an appropriate fixation system in the clinic.

* Corresponding author.
E-mail address: georg.duda@charite.de (G.N. Duda).

0268-0033/02/$ - see front matter © 2002 Elsevier Science Ltd. All rights reserved.
PII: S0268-0033(01)00102-4

In vitro experiments have been frequently employed to determine the stiffness of the bone-implant construct. Methods have been provided for the complete description of the 3D-fixation stiffness of an external stabilizer [7]. Compression, bending, and torsional tests have been performed to compare the stiffness and fatigue behavior of various plate and interlocking nail systems [8–10]. These studies provide essential information on the overall stiffness of the implant-bone construct. However, the behavior of an osteosynthesis under physiological conditions including the muscle forces remains unknown. The significance of a comprehensive understanding of the loading of long bones has been previously demonstrated [11].

The goal was to introduce a method which in addition to conventional stiffness testing allows an assessment of the suitability of a newly developed implant with regard to the loading of the implant, the bone and the tissue at the defect site. Information obtained from such an analysis is expected to delineate more clearly the indications for a new device prior to its clinical use.

2. Methods

2.1. In vitro testing

Five fresh un-matched human cadaveric tibiae without any known histories of musculo-skeletal disorders were explanted and immediately after dissection stored in a freezer until mechanical testing. Defect stabilization was performed with a new, internal fixator with locking screws (angular stability) [12] using the standard instrumentation supplied by the producer (5-hole LISS, Less Invasive Stabilization System, Synthes Bochum, Germany). An internal fixator was selected to stabilize this defect situation (Fig. 1). The internal fixator was placed on the anterio-lateral aspect of the tibia according to the manufacturer's instructions. At least three screws for each bone fragment are recommended; the necessary six holes were selected in accordance with the technical and clinical recommendation (Fig. 1). Monocortical, self-tapping and self-cutting, locking head screws (5 mm) were placed in the distal three holes of the implant. In contrast to conventional plates, the head of these screws is aligned to the body of the implant and thereby provides the screw with angular stability with respect to the implant [12]. The proximal aspect was stabilized by placing 5 mm locking head screws in the four most proximal holes of the implant. Two holes across the defect site were left empty. The defect was positioned between the first and second fifths of the tibia. Finally, stable locking of all bolts in the implant was verified and the proximal part of the bone placed in a potting jig. Using a standard methacrylate and a rectangular jig, the tibial plateau was potted such that it could be easily attached to the materials testing machine. Using an alignment jig, the tibial shaft was potted in a similar manner as the proximal aspect of the bone. Anterio-posterior and lateral radiographs were taken to verify the placement of the implants. After removal of the potting jigs, the bone was placed in the materials testing machine (Fig. 1; Zwick 1455, Germany).

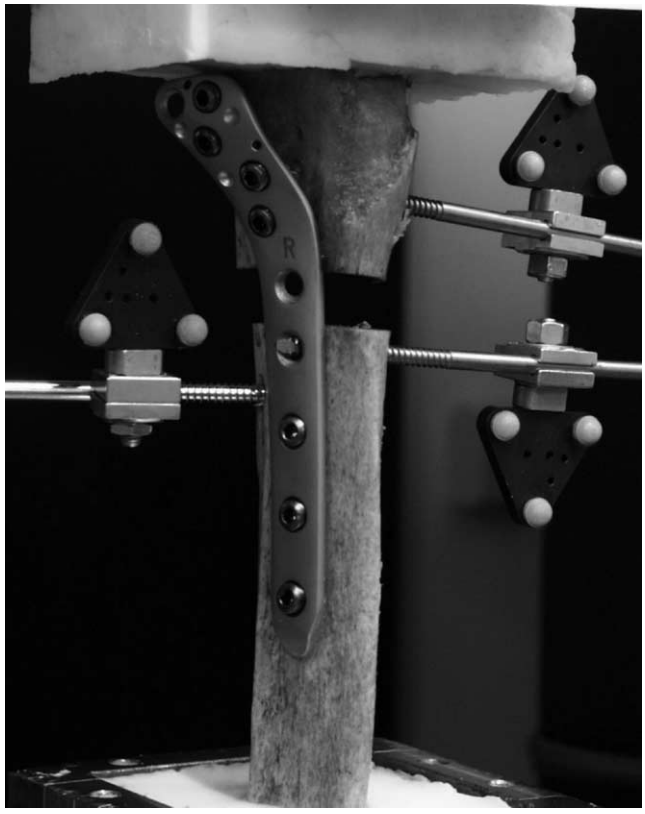

Fig. 1. In vitro compression test: Five human specimens were axially compressed and the interfragmentary movement was measured by means of an optical measurement system and triangular markers.

Two additional Schanz' screws were inserted into the bone at a distance of 1 cm from the defect gap in order to measure interfragmentary movement. Reflective markers were attached to these Schanz' screws to monitor rigid body movements by means of an optical measurement system (Fig. 1; PCReflex, Qualisys, Sweden). This system consisted of two infrared cameras, video boards and a PC for data acquisition; the 3D position of each marker was collected at a frequency of 60 Hz. The 3D offset of the triangles relative to the center of the defect gap was measured before testing. Using this offset, the relative movements were transferred from the global into a local co-ordinate system. The local co-ordinate system was positioned at the center of the defect gap. The orientation of the local co-ordinate system was identical to the tibial coordinate

system (Fig. 2). The movements of the proximal segment were reported in respect to the distal segment.

All data were transferred to a right-handed Cartesian co-ordinate system with its origin at the centroid of the tibio-calcaneal articular surface. The z-axis pointed to the most proximal point on the intercondylar eminence. The x-axis was perpendicular to a line through the most medial point on the medial malleolus and the most lateral point on the fibular notch and was oriented frontally. The y-axis was oriented laterally (Fig. 2).

Before in vitro testing, the optical system was calibrated to an accuracy of 0.05 mm using the internal LVDT of the materials testing machine (accuracy 0.001 mm). Under force control, a maximal axial force of 500 N was applied to the proximal tibia parallel to the long axis of the bone (z-axis in Fig. 2) and the rigid body movements were measured. In each specimen, the compression test was repeated five times. From the offsets and marker movements, the interfragmentary movements at the center of the defect site were computed using custom-made software [13].

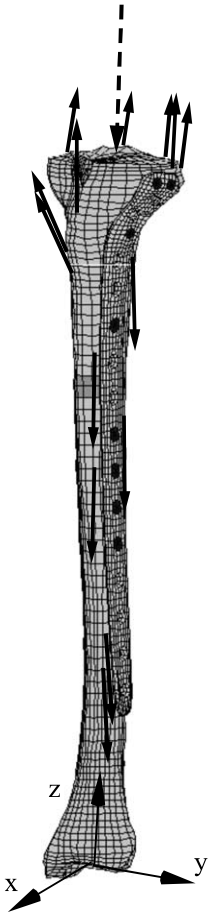

Fig. 2. Finite element model of a tibia with defect, stabilized by means of a less invasive stabilization system. The vectors represent the physiological-like loading with all muscle and joint contact forces included (Table 1). A pure compressive force – identical to the in vitro setup – was used for validation (dashed vector line).

2.2. Finite element model

The inner and outer contour profiles of the compact bone of a human tibia were identified by means of thresholding from the CT images of the Visible Human data set (National Library of Medicine, Washington, USA). The software employed for this purpose was the "Medical Image Editor" by courtesy of the German Heart Center, Berlin. CT sections were used for the proximal and distal epiphysis with a spacing of 1–2 mm and for the diaphysis with a spacing of 3 mm (Fig. 2). The treatment of horizontal defects by means of internal fixation was simulated in five independent finite element models (defects 1–5). The defect locations were evenly distributed within the proximal tibia (Fig. 6). For comparison, the straining of the intact tibia under physiological-like loading was also analyzed.

A minimum distance of 10 mm remained between any interlocking bolt and the corresponding defect line. In all instances, an 11 mm cortical deficiency simulated a mechanical worst case situation without further fragment contact. Due to the lack of fragment contact, these defects were graded in the most proximal cases as a type 41 A3 and in the shaft region as type C3 (AO classification). Injuries resulting in defect situations similar to the one modeled in this finite element analysis are complex comminuted fractures which allow no bony contact between proximal and distal segments. Such injuries are a result of a direct trauma to the proximal tibia and may be caused by a side impact of e.g., a car bumper on the tibia of a pedestrian [14]. Further, such injuries are frequently associated with a fibular fracture. Therefore, additional mechanical support by the fibula was neglected.

The geometrical properties of the less invasive stabilization system were taken from mechanical drawing data. According to the manufacturer's guidelines, a medium sized internal fixator was considered appropriate to stabilize these defects (13-hole LISS, Less Invasive Stabilization System, Synthes Bochum, Germany; Fig. 1). For defects 1–3, the internal fixator was fixed according to manufacturers guidelines such that the distal holes were left empty. For the defects 4 and 5, the whole length of the internal fixator was used (Fig. 4). The internal fixator was set at the anterio-lateral tibial aspect, according to manufacturer's instructions. At least four screws for each bone fragment were recommended; the appropriate eight holes were selected in line with clinical and technical suggestions (Fig. 4). In all defects, two holes across the defect site were left empty; the region of the internal fixator undergoing the greatest loading (working length) therefore remained unaltered. Additionally, a defect identical to defect 4 was stabilized

leaving four holes empty instead of two, thereby doubling the working length of the internal fixator.

Mesh generation relied upon the 3D surfaces of the outer and inner geometry of the intact tibia and implant geometry. 3D finite element models were generated using the TrueGrid mesh generation software (TrueGrid 1.3.23; XYZ Scientific Applications, Livermore, CA, USA). Eight-noded isoparametric brick elements were used to model cortical and trabecular bone and the internal fixator (Fig. 1). 128 brick and 387 beam elements modeled the fixation bolts.

The implant material was titanium alloy (Ti-6AL-7Nb) and modeled as linear elastic, isotropic and homogeneous with Young's modulus and Poisson's ratio of $E = 110,000$ MPa and $v = 0.30$, respectively. For the tibia, material properties were divided into three principal regions, namely, cortical bone, trabecular bone and defect site. In this first approach, the mechanical properties were assumed to be linear elastic, isotropic and homogeneously distributed [15]. In this first approach, no attempts were made to account for local changes in bone density and material properties. However, the intrinsic coupling between soft trabecular bone and rigid implant within the epiphysis might affect the loading of implant and bone. This was accounted for by a variation of Young's modulus of trabecular bone from 300 to 700 MPa within the region of implant-bone contact [15]. The material properties of the trabecular bone of the distal epiphysis were considered homogeneously distributed ($E = 700$ MPa, $v = 0.20$) [15]. The properties of the defect site were assumed to be comparable to those reported in the literature for new bone formation during the early stages of healing with extremely low Young's modulus ($E = 5$ MPa) and a rather high Poisson's ratio ($v = 0.45$) [16]. Young's modulus of the compact bone was selected to be $E = 17,000$ MPa with a Poisson's ratio of $v = 0.30$ [17,18].

2.3. Loading of the proximal tibia

In a first step, the simple axial compression test performed in the in vitro analysis was simulated in the finite element analysis. A compressive force of 500 N was applied to the tibial plateau parallel to the long axis of the tibia (z-axis in Fig. 2) resulting in interfragmentary movements at the center of the defect site.

In a second step, physiological-like loading of the intact and defect tibia was simulated. Muscle and ligament attachment data, force magnitudes and orientations were derived from the literature [11,19,20] and scaled to the tibial model [21]. Only those muscles attaching to the tibia were included as single straight lines and made to match appropriate node co-ordinates (Table 1) [22]. At the knee and ankle, joint contact forces were calculated from muscle, ligament and resultant forces. After scaling of the muscle and ligament attachments to the tibia, equilibrium of loads had to be re-established by slight variations in knee and ankle contact orientations (tilt by 3° or 4°, respectively). Fixing three nodes on the distal end of the bone restricted rigid body motions [23].

The finite element analysis was performed at an instant in gait with maximum muscle activity and high joint contact loading: before 'toe off' and at the second peak in ground reaction forces (45% of the whole gait cycle). Previous in vivo measurement of the tibial strain distribution substantiated the choice: the highest deformation of the tibia mid-shaft did in fact occur during the phase in gait between 'heel off' and 'toe off' [24]. Since this instance in time reflects a worst case scenario in mechanical terms, the behavior of the bone-implant construct was analyzed only with respect to this single instance in gait.

Loading of the implants was described by the von Mises stress along lines on their anterior and posterior edges. The von Mises stress calculation is a common representation of results in continuum mechanics and applies to ductile materials that fail under shear loading. Principal strain distribution was selected to represent the tibial load state. The interfragmentary strains were calculated in terms of relative displacements of the element nodes across the defect site; the maximum values of the corresponding strains in shear and compression were summarized in diagrams for the different defect locations.

All calculations were run using the Marc/Mentat package (Marc K72/Mentat 3.2; Marc Analysis Research Corp., Palo Alto, CA, USA) on a Unix workstation in linear elastic analysis (MIPS R 10000; Silicon Graphics, Mountain View, CA, USA).

3. Results

3.1. In vitro testing

In vitro compression testing lead to a complex movement between proximal and distal segment with moderate variations between individual specimens (Fig. 3). In relation to the distal segment, the proximal segment moved by mean 0.18 (SD, 0.01) mm dorsally and 0.33 (SD, 0.13) mm laterally. The defect side was compressed by mean 0.29 (SD, 0.07) mm. In the finite element analysis, relative movements of 0.15 mm dorsally, 0.27 mm laterally and a compression by 0.27 mm were calculated.

3.2. Finite element calculations

A survey of the surface strains in the tibia with internal fixator under physiological-like loading revealed only a slight variation of the bone loading pattern with respect to the intact condition (Fig. 4). Similar to the intact tibia, the highest strains were observed at the posterior cortex. The bone surface strains appeared to be reduced in a small region close to the defect (Fig. 4).

Table 1
System of forces and attachment co-ordinates employed in the analysis

Forces	Force (N)			Attachment (mm)		
	X	*Y*	*Z*	*X*	*Y*	*Z*
Gracilis m.	0.0	0.0	0.0	33.0	9.8	333.2
Sartorius m.	0.0	0.0	0.0	29.6	9.6	321.5
Semimembranosus m.	0.0	0.0	0.0	−23.8	−19.0	374.7
Semitendinosus m.	0.0	0.0	0.0	5.3	−38.0	377.4
Iliotibial tract I	−8.5	−8.8	61.3	−19.8	39.1	369.9
Iliotibial tract II	−97.4	−64.4	291.5	−27.1	28.2	370.5
Quadriceps femoris m.	13.6	−32.8	303.5	34.8	19.3	353.4
Extensor digitorum longus m.	0.0	0.0	0.0	3.1	13.4	107.1
Extensor hallucis longus m.	0.0	0.0	0.0	5.4	15.1	263.6
Flexor digitorum longus m.	0.0	0.0	0.0	−8.0	3.9	281.2
Tibialis anterior m. I	17.2	38.7	−327.7	−4.9	9.9	251.8
Tibialis anterior m. II	25.9	53.6	−191.8	−7.6	9.9	127.9
Tibialis posterior m.	0.0	0.0	0.0	−3.5	−8.9	251.4
Soleus m.	−63.1	−47.1	−679.0	−7.4	15.0	332.2
Ant. tibiofibular lig.	−132.4	−111.2	−56.8	−7.3	11.1	0.9
Ant. cruciate lig.	87.5	101.5	41.1	10.3	−5.0	390.5
Deltoid lig.	44.9	9.7	15.7	−1.5	−16.5	−0.3
Post. cruciate lig.	0.0	0.0	0.0	−6.0	6.0	388.3
Knee	232.3	214.9	−1528.1	1.5	−2.0	388.2
Ankle	−120.0	−154.4	2070.4	0.8	0.6	0.4

Components of muscle and joint contact forces and coordinates of attachment points on the surface of the tibia are reported for the second peak in ground reactions during gait (45% of gait cycle). Instead of reporting the distributed joint contact forces, the sum of ankle and knee joint contact forces are given. Muscles that are not activated show force magnitudes of "0" in *x*, *y* and *z* [22].

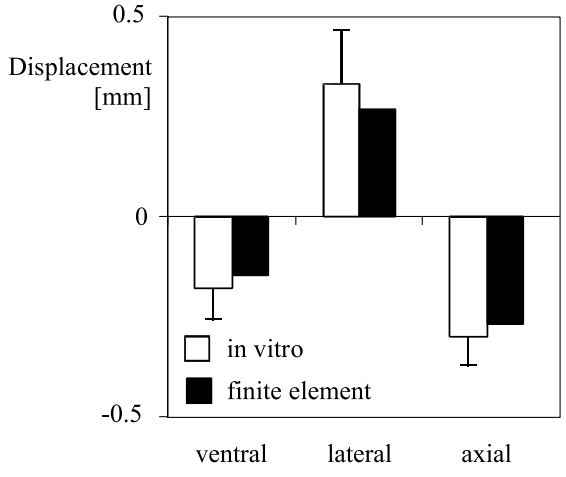

Fig. 3. Comparison between in vitro measured ($n = 5$ specimens) and calculated interfragmentary movements at 500 N.

Beyond this region, the loading seemed to resemble the intact conditions. Only for the mid-shaft defect fixation (defects 4 and 5) did the internal fixator appear to affect the bone loading pattern markedly.

Under physiological-like loading, the implant showed bending superimposed onto compression in the region bridging the defect. The maximum von Mises stresses occurred at the anterio-lateral edge of the internal fixator and increased from the proximal to the distal defect (Fig. 5). The stresses were obviously higher in the region crossing the defect. For defect 4 and especially for defect 5, the stress reached critical levels close to material failure at about 750 MPa. The bending of the implant in the region across the defect led to tilting of the proximal fragment with respect to the distal one.

Under physiological-like loading, the interfragmentary movement in shear was approximately 5% or less (Fig. 6). The compressive strains gradually increased from defect 2 to the most distal defect. Together with the axial strains, the relative tilt of the two fragments increased from the proximal to the distal defects.

Analysis of the working length of the internal fixator revealed rather large von Mises stresses for stabilization with a short working length (Fig. 7a). In contrast, the von Mises stresses were considerably lower in the internal fixator with large working length (Fig. 7b). Thus, the positioning of screws as well as the size of the working length seems to have an influence on the loading of the implant.

4. Discussion

Conventional stiffness testing allows a comparison of the stiffness characteristics of a newly developed implant with those of implants with known characteristics.

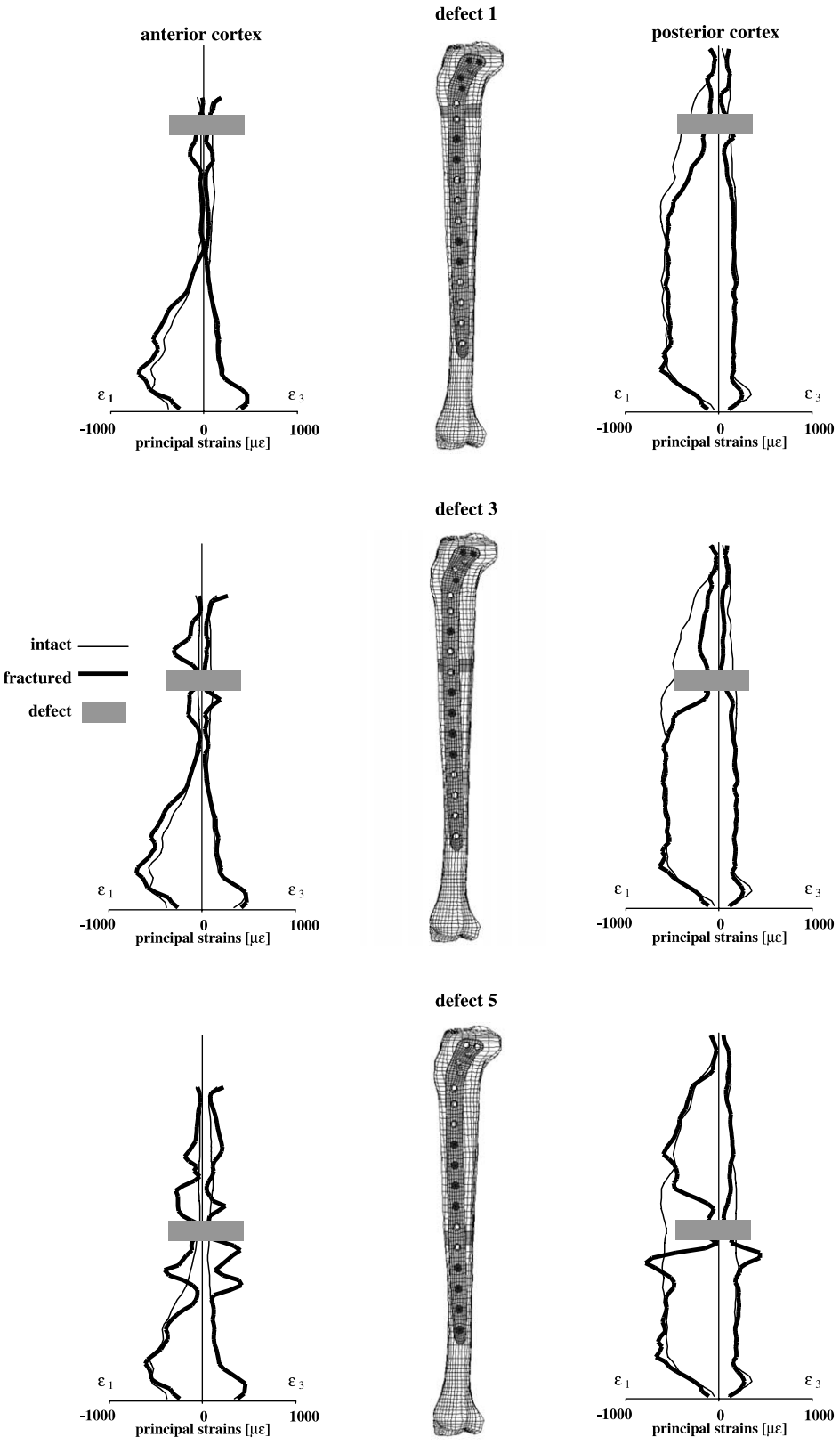

Fig. 4. Maximum (ε_1) and minimum (ε_3) principal strains along lines at the posterio-medial and anterio-lateral aspects of the stabilized tibia for the five defect locations under physiological loading.

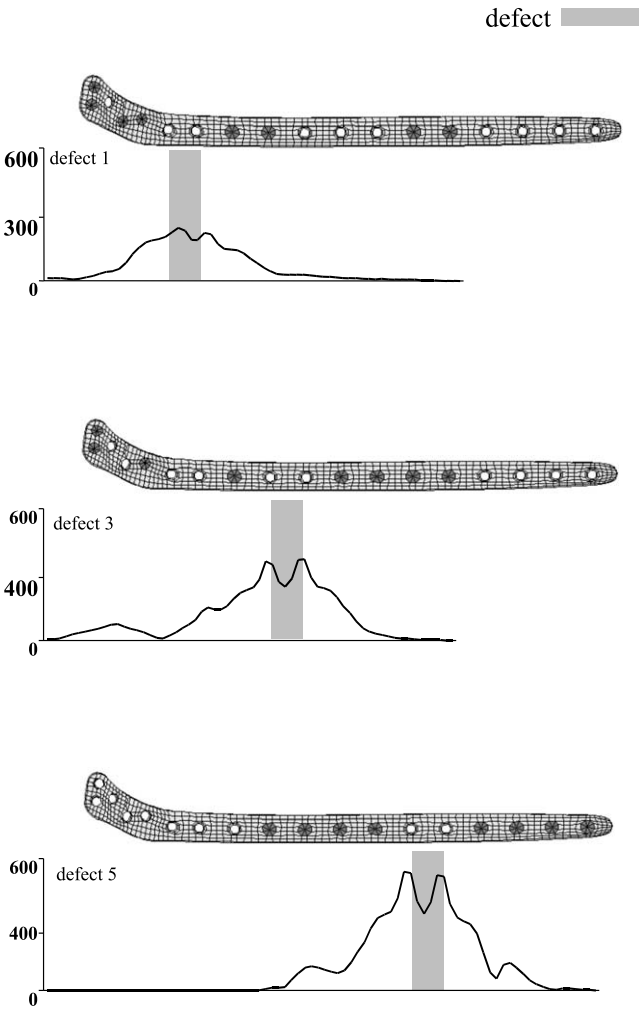

Fig. 5. Von Mises stresses on the anterior edge of the less invasive stabilization system for the five defect locations under physiological loading.

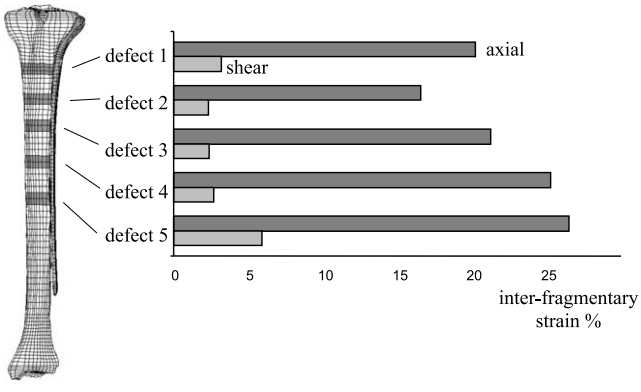

Fig. 6. Interfragmentary strains for different defect locations under physiological loading.

Usually, the intention is to compare the stiffness data with clinical experience of the analyzed implants. From this, the suitability of a new design or method of defect stabilization can be assessed. The aim of this work was

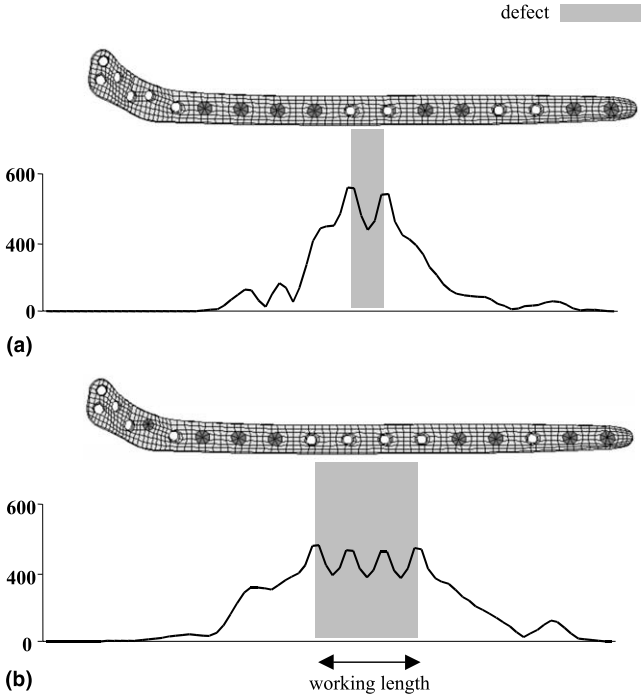

Fig. 7. Influence of the working length on the von Mises stresses on the anterior edge of the implant under physiological loading. (a) Short working length with only two holes left empty across the defect gap. (b) Long working length with four holes left empty across the defect gap.

to analyze the potential of a new approach which, in addition to conventional stiffness testing, considers physiological-like loading conditions. This allows the evaluation of the appropriateness of a newly developed implant based on knowledge of the loading of the implant, the bone and the tissue at the defect site. The information obtained from such an analysis is expected to define more narrowly the indications for a new device prior to clinical use.

The analytical data presented in this work can be validated from both in vitro as well as in vivo experimental findings. In the in vitro test, similar interfragmentary movements were found compared to those derived from the finite element calculations under pure axial compression (Fig. 3): Both orientation and magnitude of the gap movements in the in vitro experiments and the finite element analysis were comparable to each other for the selected load case. It was concluded that the finite element analysis of the osteosynthesis resembles, to some degree, the in vitro behavior (Fig. 3). However, a complete validation of the finite element model would require multiple, linearly independent load cases in vitro. Therefore, the comparability of in vitro tests and finite element analysis, by means of interfragmentary movement, may be to some degree limited. The specimen preparation and experimental usage, however, did not allow more than compression tests with these specimens to be performed.

The question remains as to what degree the calculated strains of a physiological-like loaded, intact bone may be compared to in vivo measurements in humans. The instrumentation of a bone's surface with strain gauges has made it possible to record bone deformation during various activities in animals [25] and in humans [24]. The measurements performed by Lanyon were limited to a small surface area (dimensions of the strain gauge rosette) on the antero-medial aspect of the tibial mid-shaft. The maximal deformation for normal walking occurred prior to "toe off" with a compressive maximal principal strain equal to −230 με. Similar results were obtained in this finite element analysis under physiological-like loading for the intact, not-fractured tibia with major principal strains ranging from −180 με on the anterio-lateral aspect to −300 με on the posterio-medial aspect of the bone [22]. The similarity between in vivo data and calculations for the intact tibia further supports the selection of a complex loading scenario to mimic the physiological load state in vivo. In addition to uni-axial in vitro testing, the finite element method opens up the possibility of analyzing the complex mechanical circumstances of a physiological-like load scenario.

In proximal tibial defects, only the posterior cortex showed a slight reduction in bone loading due to the defect fixation. In shaft defects, however, the bone was considerably unloaded compared to the intact situation. The loading of implant and bone seems to be more favorable in an angularly stable fixation of a proximal defect compared to a midshaft defect. In metaphyseal defects, the implant was only moderately loaded compared to the defects of the proximal shaft region. Considering the limitations of a rough finite element mesh for the implant, the analysis suggests an implant loading close to the yield strength of the material (750 MPa according to [26]) for defects of the shaft region. Even though a failure analysis of the implant needs further mesh refinement, the results show that the defect location has a considerable influence on the loading conditions of the implant and may thus affect the long-term performance of the implant. Although recent postoperative protocols limit weight-bearing for not less than 6 weeks [27–29], these results suggest that the new device would be suitable for early functional treatment of metaphyseal defects whereas in proximal shaft and midshaft defects, early weight-bearing should be restricted.

The analysis of the influence of defect location showed only minor variations on the interfragmentary strain for metaphyseal defects and defects of the proximal shaft. This is in contrast to an earlier study on unreamed nailing, which showed a considerable difference between interfragmentary strains for various defect situations [22]. However, the relatively small variation in interfragmentary strains for different defect locations might be due to the limited sensitivity analysis employed in this finite element study. Considerable axial interfragmentary strains were evident at all metaphyseal and diaphyseal defect locations for an initial defect situation with no bone formation or healing taking place. These initial strain magnitudes corresponded to the initial strains reported to be optimal from animal experiments [2,30]. However, it should be considered that mechanical straining, reported to show optimal healing results in animals, may not be transferable directly to the human situation of defect healing. The stability provided by the internal fixation system led to a relatively small amount of shear compared to the axial movement component. This is in contrast to an unreamed nail which results in a large amount of shear compared to the axial movement component [22].

An increase in working length (4 versus 2 holes left empty between defect fragments) led to a considerable reduction in implant loading. With increasing working length the implant-bone-construct became less stiff in compression and bending and the stresses in the implant itself were reduced. Since the modeling of the implant and the implant-bone interface was rather simplistic, the results represent a first estimate. However, the analysis reveals the importance of the screw positioning for the loading of the implant itself.

The angularly stable fixation in the less invasive stabilization system is based on the concept of an internal fixator, which leaves the defect zone untouched. The implant simply bridges this region whilst allowing stability of the fragments. As suggested by the findings in this study, the concept of an internal fixator has mechanical limitations as well as biological advantages: The analytical findings of this study suggest that the mechanical properties of this new device are advantageous in metaphyseal tibial defects, whereas the less invasive stabilization system should be used with care in defects of the proximal shaft. In all instances possible, a sufficient working length should be allowed between defect fragments such that implant loading remains within safe limits.

In addition to stiffness testing, the finite element analysis, under physiological-like loading, illustrates the appropriateness of this new device for the treatment of proximal defects of the tibia although the implant should not be used indiscriminately in fractures or defects extending into the diaphyseal region of the bone. This new analytical approach helped to identify clinical indications for the implant which are advantageous due to their mechanical characteristics under physiological-like loading conditions. This information was more readily obtained than it could have been with conventional testing alone. It is suggested that new implant designs be optimized, not only in respect to their in vitro stiffness but also in respect to their behavior under physiological-like loading conditions.

Acknowledgements

The authors would like to acknowledge the contributions of Dr. Michael Schütz, Trauma and Reconstructive Surgery, Charité and Dr. Jörg Goldhahn and Markus Hehli, AO Development Institute, Davos. Further, the authors would like to thank Prof. Dr. Richard Brand, Orthopedic Biomechanics Laboratory, The University of Iowa for providing the anatomical and muscle force data. Thanks to Mr. Klaus Dannenberg for developing the in vitro test set-up and to Prof. Dr. Stephan Perren, AO Research Institute, Davos and Dr. William Taylor, Trauma and Reconstructive Surgery, Charité for editing.

This project was supported by a grant from the AO ASIF Foundation, Switzerland.

References

[1] Haas N, Schütz M, Südkamp N, Hoffmann R. The new unreamed AO nails for the tibia and the femur. Acta Orthop Belg 1995;61(Suppl. 1):204–6.
[2] Claes L, Wilke H-J, Augat P, Rübenacker S, Margevicius KJ. Effect of dynamization on gap healing of diaphyseal fractures under external fixation. Clin Biomech 1995;10:227–34.
[3] Goodship AE, Kenwright J. The influence of induced micromovement upon the healing of experimental tibial fractures. J Bone Joint Surg, Br 1985;67:650–5.
[4] Kenwright J, Richardson JB, Cunningham JL, et al. Axial movement and tibial fractures. A controlled randomized trial of treatment. J Bone Joint Surg, Br 1991;73:654–9.
[5] Kenwright J, Goodship AE. Controlled mechanical stimulation in the treatment of tibial fractures. Clin Orthop 1989;241:36–47.
[6] Turner CH, Anne V, Pidaparti RMV. A uniform strain criterion for trabecular bone adaptation: Do continuum-level strain gradients drive adaptation? J Biomech 1997;30:555–63.
[7] Duda GN, Kirchner H, Wilke H-J, Claes L. A method to determine the 3D stiffness of fracture fixation devices and its application to predict inter-fragmentary movement. J Biomech 1998;31:247–52.
[8] Schandelmaier P, Krettek C, Tscherne H. Biomechanical study of nine different tibia locking nails. J Orthop Trauma 1996;10:37–44.
[9] Lewis G, Holland D. Geometrical properties and torsional fatigue life of a tibial interlocking intramedullary nail segment. J Orthop Trauma 1998;12:8–15.
[10] Fankhauser C, Frenk A, Marti A. A comparative biomechanical evaluation of three systems for the internal fixation of distal femur fractures. Trans Orthop Res Soc 1999;1:498.
[11] Duda GN, Heller M, Albinger J, et al. Influence of muscle forces on femoral strain distribution. J Biomech 1998;31:841–6.
[12] Haas N, Schütz M, Hoffmann R, Südkamp N. LISS – Ein neuer Fixateur intern für distale Femurfrakturen. OP J 1997;3:340–4.
[13] Duda GN, Kassi J-P, Hoffmann JE, et al. Mechanical behavior of Ilizarov ring fixators. Effect of frame parameters on stiffness and consequences for clinical use. Unfallchirurg 2000;103:839–45.
[14] Krettek C, Schandelmaier P, Rudolf J, Tscherne H. Current status of surgical technique for unreamed nailing of tibial shaft fractures with the UTN (unreamed tibia nail). Unfallchirurg 1994;97:575–99.
[15] Hayes WC, Swenson Jr. LW, Schurman DJ. Axisymmetric finite element analysis of the lateral tibial plateau. J Biomech 1978;11:21–33.
[16] Claes LE, Heigele CA. Magnitudes of local stress and strain along bony surfaces predict the course and type of fracture healing. J Biomech 1999;32:255–66.
[17] Evans FG. Mechanical properties of bone. Springfield, IL: Charles C. Thomas; 1973.
[18] Little RB, Wevers HW, Siu D, Cooke TD. A three-dimensional finite element analysis of the upper tibia. J Biomech Eng 1986;108:111–9.
[19] Brand RA, Crowninshield RD, Wittstock CE, et al. A model of lower extremity muscular anatomy. J Biomech Eng 1982;104:304–10.
[20] Brand RA, Pedersen DR, Friederich JA. The sensitivity of muscle force predictions to changes in physiological cross-sectional area. J Biomech 1986;19:589–96.
[21] Sommer HJ, Miller NR, Pijanowski GJ. Three-dimensional osteometric scaling and normative modelling of skeletal segments. J Biomech 1982;15:171–80.
[22] Duda GN, Mandruzzato F, Heller M, et al. Mechanical boundary conditions of fracture healing: Borderline indications in the treatment of unreamed tibia nailing. J Biomech 2001;34:639–50.
[23] Heller M, Mandruzzato F, Hehli M, et al. Importance of muscle forces on the loading of fractured tibia after unreamed nailing. Trans Eur Orthop Res Soc 1999;1:O8.
[24] Lanyon LE, Hampson WGJ, Goodship AE, Shah JS. Bone deformation recorded in vivo from strain gauges attached to the human tibial shaft. Acta Orthop Scand 1975;46:256–68.
[25] Lanyon LE, Smith RN. Measurements of bone strain in the walking animal. Res Vet Sci 1969;10:93–4.
[26] Steinemann SG, Mäusli P-A, Szmukler-Moncler S, et al. Beta-Titanium alloy for surgical implants. Titanium '92, Sci Technol 1993;1:2689–96.
[27] Schandelmaier P, Krettek C, Rudolf J, Kohl A, Tscherne H. Advantages of the unreamed tibial nail in comparison with external fixator in treatment of grade 3 B open tibial shaft fractures. Unfallchirurg 1997;100:286–93.
[28] Ostermann PA, Hahn M, Ekkernkamp A, Neumann K, Muhr G. Monocondylar fractures of the femur. Therapeutic strategy and clinical outcome. Chirurg 1997;68:72–6.
[29] Ruchholtz S, Nast-Kolb D, Betz A, Schweiberer L. Fracture healing after intramedullary nailing of simple tibial shaft fractures. A clinical comparison of reamed and unreamed procedures. Unfallchirurg 1995;98:369–75.
[30] Augat P, Margevicius K, Simon J, et al. Local tissue properties in bone healing: influence of size and stability of the osteotomy gap. J Orthop Res 1998;16:475–81.